crystals

MDPI

Article

Study on the Characteristics of Crystal Formation and Transformation of Alkali-Activated Slag Minerals Induced by Weak Alkali

Guodong Huang [1,2,*], Yonghao Huang [1], Xiaojun Zheng [3], Fengan Zhang [4], Jiahao Xu [1], Jun Qi [1] and Zijian Chen [1]

[1] School of Civil Engineering and Construction, Anhui University of Science and Technology, Huainan 232001, China; hangyonghao@aust.edu.cn (Y.H.); xujiahao@aust.edu.cn (J.X.); qijun@aust.edu.cn (J.Q.); chenzijian@aust.edu.cn (Z.C.)
[2] Institute of Environment-Friendly Materials and Occupational Health, Anhui University of Science and Technology, Wuhu 241003, China
[3] China Construction Second Engineering Bureau Co., Ltd., Beijing 100160, China; zhengxiaojun@aust.edu.cn
[4] Special Equipment Inspection Institute of Anhui, Hefei 230051, China; zhangfengan@aust.edu.cn
* Correspondence: hgd522500@163.com

Abstract: Strong-alkali activation is a prerequisite needed to ensure the full polymerization activity of alkali slag binder and establish excellent mechanical properties; however, it substantially increases the preparation cost. In this study, the effects of both strong and weak alkaline activators on the activation performance of alkali slag were examined, using a combination of X-ray diffraction, scanning electron microscopy, and Fourier-transform infrared spectroscopy analysis methods. The reaction mechanism was analyzed under different alkaline conditions, and the preparation cost could be significantly reduced without significantly degrading mechanical properties. The results indicate that $Ca(OH)_2$ can stimulate the reactivity of slag, resulting in a 40% decrease in compressive strength (compared to NaOH) but a 25–50% reduction in preparation cost. With increasing $Ca(OH)_2$ dosage, the compressive strength first increases and then decreases. The best excitation effect is achieved at a dosage of 40 g $Ca(OH)_2$ per 450 g GBFS. The formation of aluminosilicate is the main driving force for the observed increase in compressive strength. Excessive dosage of $Ca(OH)_2$ will lead to its deposition in the specimen, thus affecting the development of compressive strength.

Keywords: alkaline activation; granulated blast furnace slag; compressive strength; activator; $Ca(OH)_2$

check for updates

Citation: Huang, G.; Huang, Y.; Zheng, X.; Zhang, F.; Xu, J.; Qi, J.; Chen, Z. Study on the Characteristics of Crystal Formation and Transformation of Alkali-Activated Slag Minerals Induced by Weak Alkali. *Crystals* **2024**, *14*, 1086. https://doi.org/10.3390/cryst14121086

Academic Editor: Vladislav V. Gurzhiy

Received: 22 November 2024
Revised: 13 December 2024
Accepted: 14 December 2024
Published: 17 December 2024

Copyright: © 2024 by the authors. Licensee MDPI, Basel, Switzerland. This article is an open access article distributed under the terms and conditions of the Creative Commons Attribution (CC BY) license (https://creativecommons.org/licenses/by/4.0/).

1. Introduction

Granulated blast furnace slag (GBFS) is an industrial solid waste generated during the smelting of pig iron in blast furnaces. After ball milling treatment, GBFS has potential polymerization reaction activity, and under strong-alkali stimulation, GBFS can exhibit excellent cementitious properties [1]. Alkali-activated GBFS has superior early and high strength characteristics [2]. It also offers advantages in durability [3,4]. The most important advantage is that the carbon emissions of alkali-activated GBFS are only 25–50% of those of cement-based materials, and the energy consumption for preparation is even 40–80% lower than that of the latter [5]. Therefore, alkali-activated GBFS is hailed as the new, low-carbon, energy-saving, and environmentally friendly building material most likely to replace cement in the 21st century [6].

With deepening research, scholars have found that alkali-activated GBFS also presents serious challenges. Examples of these challenges are its high shrinkage rate (usually six times that of cement-based materials), rapid carbonation rate, and the possibility to induce alkali aggregate reactions [7–9]. Shi, Zhang, and others [10,11] studied the alkaline activation ability of Na_2CO_3, NaOH, and sodium silicate mixed alkali components on GBFS. Research has shown that high concentrations of OH^- can accelerate slag hydration, promote

the formation of both silicates and aluminosilicates, and, thus, accelerate solidification. Nasr et al. [12]. studied the influence of activator concentration and curing conditions on atomic absorption spectrometry performance. They found that the curing temperature positively impacts the atomic absorption spectrometry performance, while the effect of an increased activator concentration is not significant. Zheng et al. [13]. studied the influence of different types of activators on the performance of alkali slag mortars. Their results indicate that high sodium hydroxide and sodium carbonate contents positively affect mechanical property.

Scholarly research has mainly focused on the excitation effects of activators and their impact on mechanical and durability properties [14]. However, the most critical issue with alkali-activated GBFS is that suitable strength can only be established under strong-alkali activation [15]. However, the use of activators such as NaOH and liquid sodium silicate substantially increases the preparation cost (about 1.5–2 times that of cement-based materials), thus imposing the main bottleneck restricting the large-scale engineering application of alkali-activated GBFS [16]. Therefore, how to significantly reduce the preparation cost without significantly reducing the mechanical properties is the key issue studied in this article.

This paper focuses on the key scientific issue of designing and regulating the mixing proportion of high-performance slag activated by weak alkali. A specific emphasis is placed on analyzing the polymerization reaction mechanism, mechanical property development laws, and impact on the microstructure of alkali-activated GBFS under different weak-alkali activation conditions; the results are compared and contrasted with those of strong-alkali activation conditions. Finally, a composition design method for preparing alkali-activated GBFS with controllable mechanical properties and an adjustable setting time using weak alkali is proposed. The proposed method substantially reduces the preparation cost and promotes the engineering application of low-cost, high-performance, low-carbon, energy-saving, and environmentally friendly alkali-slag materials.

2. Experimental Materials and Methods

2.1. Experimental Materials

2.1.1. GBFS

S95-grade GBFS [17] provided by a certain mineral product company in Lingshou County, Hebei Province, China was used. This GBFS had a specific surface area of 400 m^2/kg, a 45 μm square hole sieve residue of 5%, and chemical composition as shown in Table 1.

Table 1. Physical and chemical properties of materials %.

	Specific Surface Area (m^2/kg)	Square Hole Sieve Residue (45 μm %)	CaO	SiO_2	Al_2O_3	Fe_2O_3	MgO	Na_2O	K_2O	Others	LOI
GBFS	400	5	35.57	32.26	19.23	0.98	7.46	0.13	0.42	1.85	1.72

2.1.2. Stimulating Agents

As activators, NaOH, $Ca(OH)_2$, and Na_2CO_3 were used, all of which were of analytical grade and were provided by a certain technology company in Langfang, Hebei, China. NaOH was dissolved in water for activation, while $Ca(OH)_2$ and Na_2CO_3 were directly added to GBFS for activation. The specific dosages and method of addition are shown in Table 2 and described in Section 2.2.2.

Table 2. Mixing proportion design.

	GBFS	NaOH(N)	$Ca(OH)_2$(C)	Na_2CO_3(S)	Water	Sand	Paste pH
N0	450	0	0	0	225	1350	9.33
N20	450	20	0	0	225	1350	14.35
N40	450	40	0	0	225	1350	14.65
C20	450	0	20	0	225	1350	12.85
C40	450	0	40	0	225	1350	12.95
C60	450	0	60	0	225	1350	12.96
S20	450	0	0	20	225	1350	11.45
S40	450	0	0	40	225	1350	11.51
S60	450	0	0	60	225	1350	11.52

Note: The pH values of N20 and N40 are calculated.

2.2. Experimental Methods

2.2.1. Mixing Proportion Design

The experimental procedure is presented in Table 2. The cementitious materials were all made of GBFS, and the dosage was maintained at 450 g. N0 did not contain any activator and was used to test the polymerization activity of GBFS under free-water condition. From N20 to N40, the dosage of NaOH gradually increased and the development law of polymerization reaction activity and mechanical properties of GBFS excited by strong alkali were analyzed. The influence of weak bases on the activity and mechanical properties of GBFS polymerization reaction was analyzed in depth; C20–C60 and S20–S60 were excited using $Ca(OH)_2$ and Na_2CO_3, respectively.

2.2.2. Preparation and Curing of Mortars

First, a mixer was used to mix GBFS and $Ca(OH)_2$ evenly according to the ratio presented in Table 2 (C20). Then, both constituents were placed in a mixer and experimental water was added, followed by quick stirring for 30 s and addition of sand, again followed by further quick stirring for 60 s. Then, the pH of the mixed slurry was measured (pH meter) and the result was recorded in Table 2. Finally, the mixture was poured into a 40 mm × 40 mm × 160 mm mold and vibrated to remove air bubbles. The preparation of other specimens carried out in accordance with C20. At 24 h, the mold was removed, and curing continued at a temperature of 20 °C and a humidity of 98%.

2.2.3. Analysis of Compressive Strength

A DYE-300S fully automatic cement mortar testing machine (Honghao Jieke Construction Instrument Co., Ltd., Cangzhou, Hebei, China) was used to test the compressive strength of specimens after 1 day, 3 days, 28 days, and 60 days of curing (GB/T 17671-2021) [18]. The influence of the type and dosage of the activator on the development law of alkali slag strength was analyzed.

2.2.4. Microscopic Analysis

Microscopic analysis was conducted using X-ray diffraction (XRD) (RIGAKU, Tokyo, Japan), Fourier-transform infrared spectroscopy (FT-IR) (Nicolet is50, Washington, DC, USA), and scanning electron microscopy (SEM) (FlexSEM1000, Tokyo, Japan). The influence of different weak alkali and dosages on the condensation polymerization and transformation characteristics of alkali GBFS mineral gels, as well as the evolution of both microstructure and chemical structure, were examined. The instruments used were the Rigaku Smartlab X-ray diffractometer from the Analysis and Testing Center of Anhui University of Science and Technology, the Nicolet is50 Fourier Transform Infrared Spectrometer from Thermo Fisher Scientific in Waltham, MA, USA, and the FlexSEM1000 desktop scanning electron microscope from Hitachi in Tokyo, Japan.

3. Results and Analysis

3.1. Analysis of Compressive Strength

3.1.1. Analysis of Compressive Strength Under Free Water

Figure 1 shows the development law of compressive strength of alkali-activated GBFS specimens under different excitation conditions. Specimen N0 (water excited) could not be demolded after 3 days of curing, and its compressive strength only reached 1.4 MPa after 28 days of curing. With continuing curing, a significant increase in compressive strength was still not observed after 60 days. This result shows that free water cannot stimulate the polymerization reaction activity of GBFS, and the specimen could not establish and develop compressive strength. When GBFS was mixed with free water, the pH of the mixed slurry was only 9.33. Weak-alkali stimulation cannot promote the depolymerization of ionic compound and dissolution of active ions in GBFS [19]. Moreover, there is a lack of sufficient power to stimulate the re-aggregation of active ions in the reaction slurry, which, thus, cannot form high-strength silicate and aluminate gels [20]. This leads to the observation that compressive strength cannot be established and developed in this specimen.

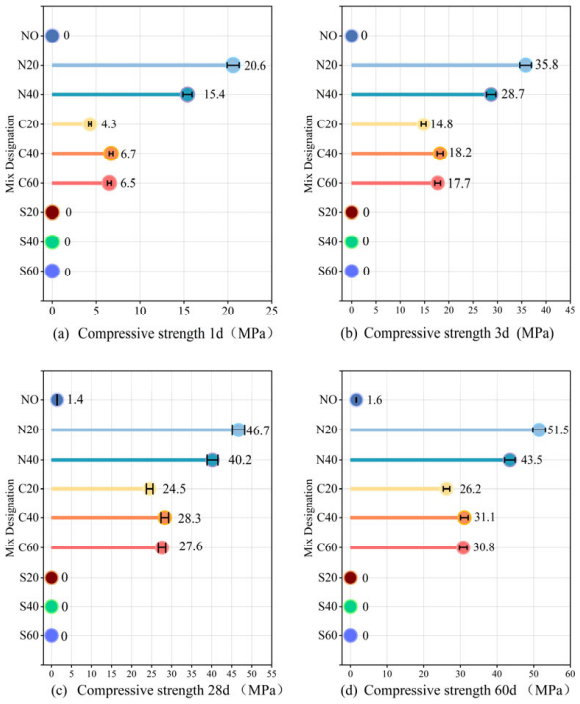


Figure 1. Analysis of NaOH-, $Ca(OH)_2$-, and Na_2CO_3-induced compressive strength.

3.1.2. Analysis of NaOH-Induced Compressive Strength

At a dosage of NaOH of 20 g, the N20-cured specimen reached 20.6 MPa after 1 day of curing, which increased to 35.8 MPa after 3 days, exhibiting excellent early strength and high strength characteristics. After 28 and 60 days of curing, the compressive strength increased substantially to 46.7 MPa and 51.5 MPa, respectively. When GBFS was mixed with NaOH solution, the pH of the mixed slurry increased to 14.35 (Table 2). Strong alkaline excitation conditions effectively promote the depolymerization of ionic compound in GBFS, accelerate dissolution and polymerization, promote the formation of condensation products, and increase the polymerization reaction rate [21]. NaOH solution could effectively stimulate the polymerization reaction activity of GBFS and promote both the establishment and development of strength [22].

At an NaOH dosage of 40 g, the compressive strength of specimen N40 decreased to varying degrees at different curing ages. Compared with specimen N20, these decreases ranged between 15% and 20%. Although the pH of the mixed slurry of specimen N40 increased to 14.65 (Table 2), the compressive strength decreased substantially. This result

shows that although an increase in pH is beneficial for the depolymerization, dissolution, and re-polycondensation of active ions in GBFS, it can also further improve the polymerization rate. However, an excessively high pH is not conducive to the formation of calcium silicate hydrate gel, but it leads to the instability of calcium silicate hydrate gel [23]. Excessive Na^+ actively combines with Al^{3+} to replace Ca^{2+} in calcium silicate hydrate gel; consequently, the high-strength calcium silicate hydrate gel can be transformed into low-strength sodium aluminosilicate gel [24], which is the reason why increasing the amount of NaOH leads to a reduction in compressive strength.

3.1.3. Analysis of $Ca(OH)_2$-Induced Compressive Strength

When stimulated with $Ca(OH)_2$, the strength of specimen C20 after 1 day and 3 days of curing reached 4.3 MPa and 14.8 MPa, which were 79.1% and 58.7% lower than the strength of specimen N20, respectively. After 28 and 60 days of curing, the strength of specimen C20 increased to 24.5 MPa and 26.3 MPa, which were 47.5% and 49.1% lower than that of specimen N20, respectively. While $Ca(OH)_2$ can stimulate the polymerization activity of GBFS, the early compressive strength is insufficient, and later strength growth is apparent. The overall activation effect is substantially weaker than that of NaOH. The pH of C20 mixed slurry is only 12.85, which severely affects the reaction process of active ingredients in GBFS; it also hinders the formation of high-strength calcium silicate and calcium aluminosilicate gels and leads to an apparent lack of early compressive strength [25]. During the later maintenance process, $Ca(OH)_2$ can continue to dissolve (because of its slight solubility characteristic), thereby compensating for the continuous consumption and loss of OH^- during the polymerization reaction [26]. This ensures that the pH inside the specimen is maintained at 12.85, thereby effectively maintaining the alkaline excitation power. This maintenance of the strength of specimen C20 continued to substantially improve in the later stage.

When the dosage of $Ca(OH)_2$ was increased to 40 g, the pH of the mixed slurry increased to 12.95. The strength of specimen C40 after 1 day and 3 days of curing increased to 7.8 MPa and 19.2 MPa, which was 81.4% and 29.7% higher than the strength of specimen C20, respectively. When cured for 28 and 60 days, the strength of specimen C40 increased to 29.3 MPa and 32.1 MPa, which exceeded the strength of specimen C20 by 19.6% and 22.5%, but was 37.3% and 37.7% lower compared to N20, respectively. Increasing the $Ca(OH)_2$ content not only maintains the internal alkaline environment, but also provides more active Ca^{2+} for the polymerization environment. Active calcium is an important component of the condensation that forms calcium silicate gel and calcium aluminosilicate gel. Thereby, active calcium substantially improves the polymerization efficiency and promotes the formation of high-calcium gels [27]. More importantly, $Ca(OH)_2$ provides active Ca^{2+} to the reaction solution through dissolution. As Ca^{2+} continues to be polymerized and consumed, $Ca(OH)_2$ continues to dissolve, continuously replenishing the reaction solution with Ca^{2+}. This replenishment creates a calcium-rich excitation environment for the polymerization reaction, which is conducive to the formation of high-calcium polymerization products [28]. Therefore, the power and efficiency of Ca^{2+} provided by $Ca(OH)_2$ are far greater than those of GBFS depolymerization and dissolution processes. Therefore, the strength of specimen C40 continues to increase with increasing $Ca(OH)_2$ dosage. From an economic perspective, the market sales price of $Ca(OH)_2$ is only 20% of that of NaOH, and the cost of activating GBFS with $Ca(OH)_2$ only ranges between 25% and 50% of that activated by NaOH. Therefore, the use of $Ca(OH)_2$ reduces the preparation cost of alkali-activated GBFS to between 40% and 80% of that of cement-based materials. Compared with NaOH stimulation, although $Ca(OH)_2$ may result in a nearly 40% loss in compressive strength, its mechanical properties can meet the requirements for non-load bearing construction.

When the dosage of $Ca(OH)_2$ was increased to 60 g, the pH of the mixed slurry no longer increased significantly, and the compressive strength of specimen C60 at different curing ages showed varying degrees of decrease (compared to specimen C40), with a decreased range of 10–15%. Although increasing the $Ca(OH)_2$ dosage continuously can

improve the active calcium content in the reaction solution, the formation of polymerization products does not increase continuously. This is because the formation of high calcium gels also requires the condensation of active silicon and aluminum. Silicon and aluminum only come from GBFS, and as the GBFS content has not been increased, an excess of $Ca(OH)_2$ remains inside the specimen [29]. $Ca(OH)_2$ has low self-gelling ability, leading to a decrease in the compressive strength.

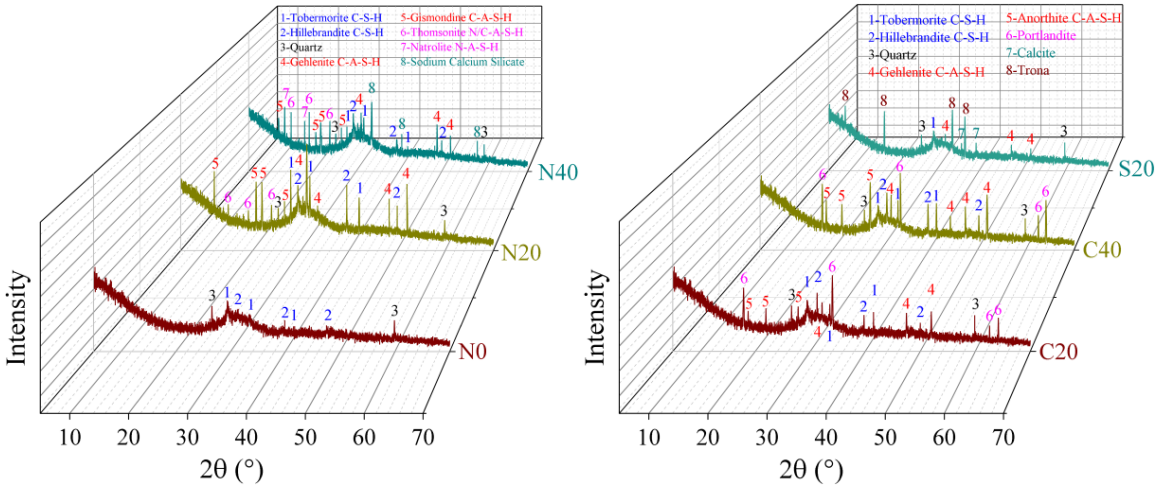
3.1.4. Analysis of Na_2CO_3-Induced Compressive Strength

Under the condition of Na_2CO_3 stimulation, specimens S20, S40, and S60 did not have a measurable compressive strength (as shown in Figure 1). Even with an increase in Na_2CO_3 content or an extension of curing time, the compressive strength of specimens at each curing age still remained 0, indicating that Na_2CO_3 could not stimulate the polymerization activity of GBFS. However, compared with the free-water-excitation condition, specimen N0 (pH = 9.33) had an extremely low compressive strength after 60 days of curing, while the pH of the Na_2CO_3-excitation condition reached 11.5; this pH value substantially exceeds the pH of the free water, and compressive strength could not be established. This result indicates that Na_2CO_3 and GBFS can undergo a polymerization reaction, but their ability to form polymerization products is too low to establish strength [30].

3.2. XRD Analysis

3.2.1. Free-Water-Induced XRD Analysis

The results of the XRD analysis of GBFS excited by free water are presented in Figure 2a. No high-intensity diffraction characteristic peaks were observed in specimen N0, and only a small number of weak characteristic peaks of tobermorite (represented by 1, $5CaO{\cdot}6SiO_2{\cdot}5H_2O$, PDF 46-1448) and hillebrandite (represented by 2, $CaSi_2O_5{\cdot}2H_2O$, PDF 42-0538) could be observed. The mineral crystallinity was poor, and the formation amount was insufficient. Additionally, few quartz crystal characteristic peaks (represented by 3) were observed. Under the condition of free-water excitation, the low alkaline pH (9.33) could only stimulate the polymerization of the active calcium and free silicon on the surface of GBFS to generate a small amount of calcium silicate hydrate gel; however, this could not enable the ionic compound inside GBFS to undergo depolymerization, dissolution, and polycondensation [31]. Therefore, the characteristic peak of specimen N0 is not apparent, and also proves the mechanism of the insufficient compressive strength of specimen N0.



(**a**) NaOH excitation (**b**) $Ca(OH)_2$ excitation

Figure 2. XRD analysis.

3.2.2. NaOH-Induced XRD Analysis

The addition of NaOH caused substantial changes in the gel crystal characteristics of specimen N20 (Figure 2a). Specimen N20 showed clear characteristic peaks of tobermorite and hillebrandite, significantly exceeding the strength of N0, indicating that a large amount of calcium silicate hydrate gel with relatively good crystallinity had formed in N20. The characteristic peak of gehlenite (represented by 4, $2CaO{\cdot}Al_2O_3{\cdot}SiO_2$, PDF 35-0755) appeared in specimen N20. Moreover, a large number of zeolite-phase characteristic peaks appeared, such as gismondine (represented by 5, $CaO{\cdot}Al_2O_3{\cdot}3SiO_2{\cdot}3H_2O$, PDF 39-1373) and thomsonite (represented by 6, $NaCa_2(Al_5Si_5O_{20}){\cdot}6H_2O$, PDF 46-1448); however, these characteristic peaks were not observed in specimen N0. Gehlenite- and gismondine-phase minerals are both calcium silicate aluminate- or sodium silicate aluminate-type minerals. Their formation proves that they can only occur under a high alkaline excitation environment [32]. The formation of high-strength silicates and aluminates is key for the early strength and high-strength mechanical properties of specimen N20.

With increasing NaOH content, the intensity of the characteristic peaks of calcium silicate gels in specimen N40 (Figure 2a) was significantly lower than that in specimen N20. This difference indicates that high NaOH content is not conducive to the polycondensation molding of calcium hydrate gel. More importantly, the intensity of the characteristic peaks of gehlenite and gismondine in specimen N40 also showed varying degrees of decrease, while the intensity of the characteristic peaks of thomsonite increased significantly. The high alkaline environment makes the calcium silicate and calcium aluminosilicate gel unstable [33]. An increase in Na^+ concentration prompts them to actively replace Ca^{2+} and form sodium-containing aluminosilicates [34]. Moreover, the appearance of the characteristic peaks of natrolite (represented by 7, $Na_2Al_2Si_3O_{10}{\cdot}2H_2O$, PDF 45-1413) and new hydrated sodium calcium silicate (represented by 8, $Na_2Ca_2Si_2O_7{\cdot}H_2O$, PDF 22-0891) in specimen N40 further proves this inference. These characteristic peaks did not appear in specimen N20. Therefore, the increase in the dosage of NaOH affects the formation of high-strength calcium silicate, resulting in the transformation of high-strength calcium silicoaluminate into low-strength sodium silicoaluminate. This transformation is the reason why the compressive strength of specimen N40 decreased.

3.2.3. $Ca(OH)_2$ Excitation XRD Analysis

The crystal characteristics of the C20 mineral excited by $Ca(OH)_2$ are shown in Figure 2b. In specimen C20, characteristic peaks of tobermorite and hillebrandite can be observed, but the intensities of these peaks are significantly lower than those of the peaks in specimen N20, and even lower than those of the peaks in specimen N40. The reason may be that the pH of $Ca(OH)_2$ is too low to establish an alkaline-excitation environment, which affects the condensation efficiency of the calcium silicate gel. Moreover, the characteristic peak of gehlenite appears in specimen C20, and the strength of the characteristic peak is also lower than the strengths of the peaks in specimens N20 and N40; this result indicates that the polycondensation of calcium aluminosilicate gel is also affected by the low pH value [35]. However, a weak characteristic peak of anorthite (represented by 5, $CaO{\cdot}Al_2O_3{\cdot}2SiO_2$, PDF 41-1486) appeared in specimen C20, but not in specimens N0, N20, and N40. This may be the result of $Ca(OH)_2$ exciting GBFS and the reason why the compressive strength of specimen C20 continued to increase. Most importantly, no zeolite-phase mineral crystal structure was observed in specimen C20, while gismondine, thomsonite, or natrolite appeared in both specimens N20 and N40. This finding indicates that only the calcium-salt or sodium-salt zeolite phase condensed and formed in high-alkaline GBFS activated by NaOH, which is also the key to the early and high strength of alkali-activated GBFS [36]. Furthermore, the characteristic peak of portlandite (represented by 6, $Ca(OH)_2$, PDF 44-1481) appeared in specimen C20, which may have been caused by the remaining $Ca(OH)_2$. Therefore, the activation effect of $Ca(OH)_2$ on GBFS is lower than that of NaOH in that it cannot form zeolite-type high-strength aluminosilicates. The

formation of tobermorite, hillebrandite, gehlenite, and anorthite ensures the continuous increase in compressive strength.

When the amount of $Ca(OH)_2$ was increased to 40 g, the characteristic peak intensities of calcium silicate gels in specimen C40 (Figure 2b) did not further increase (compared to specimen C20); however, the characteristic peaks of Calcium aluminosilicate gels followed a significant upward trend, exhibiting higher crystallinity. Increasing the $Ca(OH)_2$ content increased the active calcium content in the polymerization reaction solution and significantly improved the crystallinity of calcium aluminosilicate. This led to an increase in compressive strength but did not promote the improvement of the crystallinity of calcium silicate gel. This lack of improvement indicates that the increase in the crystallization of calcium silicate gel could only be achieved by increasing the pH of the reaction solution [37]. Moreover, the intensity of the characteristic peak of $Ca(OH)_2$ in specimen C40 also increased significantly, which is related to the increase in $Ca(OH)_2$ content.

3.2.4. Na_2CO_3 Excitation XRD Analysis

When stimulated with Na_2CO_3, weak characteristic peaks of gehlenite and calcite (represented by 7) appeared in specimen S20 (Figure 2b), and mineral characteristic peaks of trona (represented by 8, $Na_2CO_3{\cdot}NaHCO_3{\cdot}2H_2O$, PDF 22-1447) were also detected. As the pH of Na_2CO_3 in the excitation environment is low (11.45), the fracture energy required for the depolymerization of calcium oxygen, silicon oxygen, and aluminum–oxygen bonds in the GBFS cannot be reached (pH > 12) [38]. Only the polymerization of free active ions on the GBFS surface can be promoted, resulting in poor crystallinity of the calcium aluminosilicate gel. This is the reason why the characteristic peak of gehlenite is clearly insufficient. The addition of Na_2CO_3 introduces CO_3^{2-} into system, which polymerizes with calcium to form calcite. However, because of the low pH, the polymerization energy is insufficient, seriously affecting the crystallinity of calcite [39]. Moreover, the residual Na_2CO_3 in specimen S20 lead to the emergence of trona. Therefore, Na_2CO_3-activated GBFS cannot form high-strength tobermorite or hillebrandite silicates, nor can it excite high-strength silicate minerals such as zeolites. Only gehlenite and calcite with poor crystallinity can form. This is the reason why Na_2CO_3 activated GBFS cannot establish strength.

3.3. SEM Analysis

3.3.1. SEM Analysis Stimulated by Free Water

The results of the SEM analysis of GBFS excited by free water are shown in Figure 3a. A large number of GBFSs are visible in the microstructure of specimen N0. This indicates that the involvement of GBFS in the reaction is relatively low. The particles are not tightly bonded and do not form a large-scale gel structure. Moreover, the microstructure has a considerable number of pores (indicating that no gel structure and no apparent cracks had formed), and only gel-like substances had formed on the surface of a few particles. The above phenomena indicate that the degree of polymerization reaction was low, and the amount of polymerization products was clearly insufficient [40]. This also proves that the pH of the GBFS slurry was too low (9.33) to effectively stimulate GBFS activity.

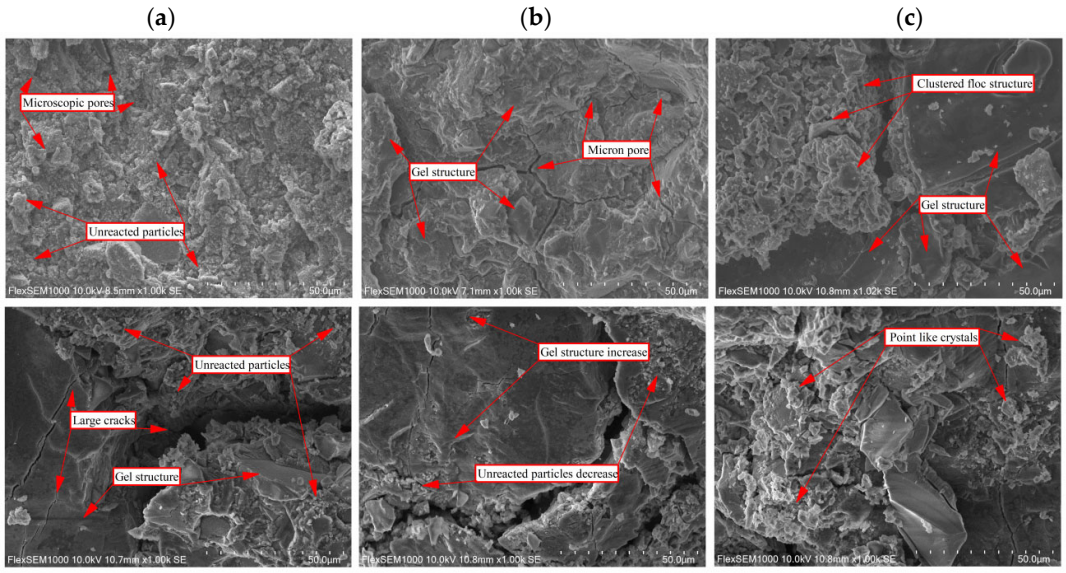


Figure 3. SEM analysis. (**a**) Specimen N0; (**b**) specimen N20; (**c**) specimen N40; (**d**) specimen C20; (**e**) specimen C40; (**f**) specimen C60.

3.3.2. NaOH-Induced SEM Analysis

The microstructure of the NaOH-stimulated specimen N20 has been significantly improved (Figure 3b), and the granular GBFS structure on the surface has almost disappeared. This result indicates that most particles participated in the polymerization reaction, forming a blocky gel structure with good integrity. The gel structure was, overall, uniform and compact, and while the number of microscopic pores decreased significantly, gel cracks appeared. The establishment of a high-alkaline excitation environment (pH = 14.35) by NaOH enabled the transformation of GBFS particles from a granular to a colloidal structure. This transformation also proves that GBFS particles themselves have good polymerization activity, but they can only be used in a high-pH environment [41].

The polymerization degree of GBFS particles in the microstructure of specimen N40 was still high (Figure 3c). Moreover, the microscopic gel structure still remained dense and uniform, but a cluster-like floc structure was found in the microstructure. This floc structure may be the generated sodium aluminosilicate [42], but it did not appear in specimen N20. Further, the floc was attached to the surface of the gel structure, leading to an increase in micro defects in the gel structure. These pores and cracks may be the reason why the compressive strength of specimen N40 decreased with increasing NaOH content.

3.3.3. $Ca(OH)_2$-Stimulated SEM Analysis

In the microstructure of $Ca(OH)_2$-activated specimen C20 (Figure 3d), a large number of GBFS particles were still observed. Only part of the GBFS particles polymerized to form a gel structure. The gel and granular GBFS were mixed together, resulting in poor integrity of the microstructure, a non-compact structure, and many cracks (Figure 3d). Because the alkaline environment established by $Ca(OH)_2$ is weak (pH = 12.85), it can only stimulate certain highly active GBFS particles to undergo depolymerization, dissolution, and re-condensation reactions [43]. The gel thus formed will wrap the unreacted GBFS particles together, which is the reason for its uneven and dense structure and apparent crack defects, as well as the reason for the insufficient mechanical properties of $Ca(OH)_2$-activated GBFS.

With an increasing amount of $Ca(OH)_2$, the microstructure of specimen C40 showed a certain improvement. Although GBFS particles could still be observed in the microstructure, their number was substantially decreased compared to those in specimen C20. Moreover, defects in the microstructure of specimen C40 have been further reduced, and the overall structure, compactness, and uniformity have improved to a certain extent. The reason for

these improvements is the effect of increasing the $Ca(OH)_2$ dosage. It not only effectively compensates for the continuous consumption of OH^- during the polymerization reaction but also supplements the loss of OH^- caused by diffusion, thereby maintaining the alkaline environment inside the specimen [44].

As the dosage of $Ca(OH)_2$ continued to increase, the microstructure of specimen C60 underwent continuous changes. GBFS particles that had not participated in the polymerization reaction still existed in the microstructure, which has not been continuously improved when compared to that of specimen C40. This indicates that the continuous increase in the amount of $Ca(OH)_2$ cannot continue to improve the degree of GBFS participation in the polymerization reaction [45]. More importantly, a large number of point-like crystals was observed in specimen C60. Although this phenomenon also occurred in specimens C40 and C20, these point-like crystal structures were more pronounced in specimen C60 and they were completely different from the flocculent structure in specimen N40. This observation may be related to the $Ca(OH)_2$ that did not participate in the polymerization reaction. With an increasing amount of $Ca(OH)_2$, the amount of $Ca(OH)_2$ remaining in specimen C60 increased gradually, and condensed in the specimen to form defects [46].

3.4. FT-IR Analysis

3.4.1. FT-IR Analysis of GBFS Excited by Free Water

The result of the FT-IR analysis of GBFS excited by free water is shown in Figure 4a. A symmetric tensile vibration of the Si–O–Si bond (represented by 1) was found at 434 cm^{-1} in specimen N0, indicating the presence of SiO_2 mineral composition. However, SiO_2 (quartz) is an inherent substance in GBFS and is not formed by the polymerization reaction [47]. A weak Si–O–T-bond (where T is tetrahedral silicon or aluminum) asymmetric tensile vibration is found at 923 cm^{-1} (represented by 2). This specific frequency is generally considered to be the characteristic of silicon oxide tetrahedron and aluminum oxide tetrahedron in calcium silicate hydrate or calcium aluminosilicate gels [48]. The strength of this characteristic peak is weak, indicating that the amount of silicate generated in specimen N0 was insufficient, which also confirms the XRD results. The CO_3^{2-} bending vibration mode appeared at 1480 cm^{-1} (represented by 5), which is related to the presence of carbonate. The characteristic peak intensity was extremely weak, indicating insufficient generation. In summary, the FT-IR analysis of GBFS excited by free water showed no substantial formation of high-strength mineral components such as silicates, aluminosilicates, or carbonates. The result was insufficient compressive strength.

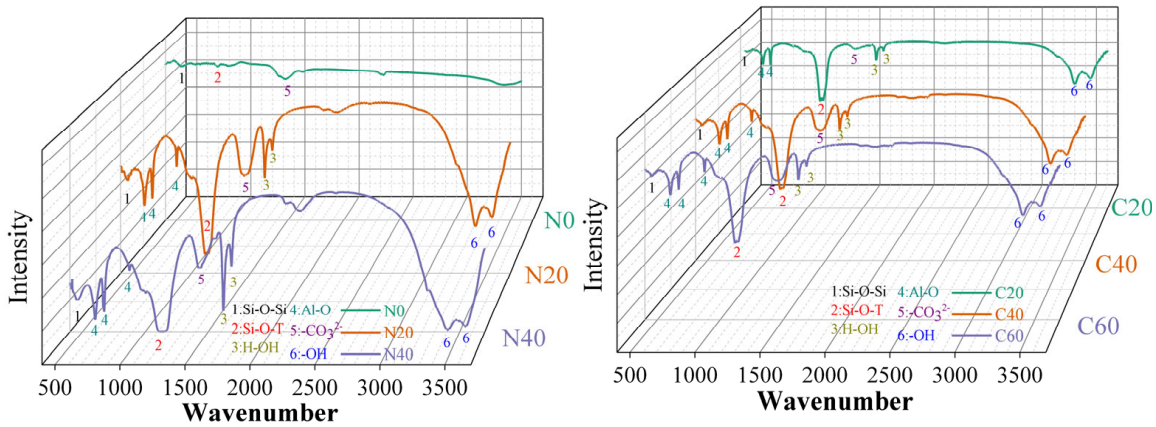


Figure 4. FT-IR analysis. (**a**) NaOH excitation; (**b**) $Ca(OH)_2$ excitation.

3.4.2. NaOH Excitation FT-IR Analysis

The FT-IR spectrum of specimen N20 (doped with 20 g NaOH) is shown in Figure 4a. An asymmetric tensile vibration of the Si–O–T bond was found at 1117 cm^{-1}, with high

characteristic peak intensity, indicating that large amounts of silicate or aluminosilicate had formed in specimen N20. At the same time, three AlO_4^- groups (represented by 4) were found to have undergone asymmetric tensile vibrations at 603 cm^{-1}, 670 cm^{-1}, and 875 cm^{-1}, indicating the formation of aluminate minerals in specimen N20. The above vibrations did not occur in specimen N0, indicating that high-strength silicates and aluminosilicates formed only under NaOH excitation conditions, which lead to an increase in the compressive strength of specimen N20 [49]. The bending vibration at 1448 cm^{-1} was significantly enhanced, indicating a substantial increase in carbonate generation (CO_3^{2-} groups). The asymmetric stretching vibrations of the H–OH bond (represented by 3) at 1621 cm^{-1} and 1686 cm^{-1} were also significantly enhanced, indicating a substantial increase in the amount of bound water. The asymmetric stretching vibrations of the -OH bond at 3404 cm^{-1} and 3546 cm^{-1} (represented by 6) increased substantially compared to that of specimen N0, which can be attributed to the addition of NaOH. Therefore, NaOH addition increased the formation of silicates, aluminosilicates, aluminates, and carbonates, which led to the substantial improvement in compressive strength. This also proves the correctness of the XRD research results.

When the NaOH content increased to 40 g, the asymmetric tensile vibration of the Si–O–T bond in specimen N40 moved from 1117 cm^{-1} to 1112 cm^{-1}, and the vibration intensity decreased, indicating the decreased formation of silicate or aluminosilicate gel. An increase in NaOH content leads to chemical changes in calcium silicate or aluminosilicate products, and the decalcification of the calcium silicate gel, thus decreasing the strength of the characteristic peak [50]. The asymmetric stretching vibration intensities of AlO_4^- groups at 671 cm^{-1} and 875 cm^{-1} were significantly reduced, indicating that calcium aluminosilicate also underwent similar decalcification. The asymmetric stretching vibration of H–OH bonds at 1621 cm^{-1} and 1684 cm^{-1} was significantly enhanced, indicating a further increase in the amount of bound water. The asymmetric stretching vibrations of the -OH bond at 3402 cm^{-1} and 3543 cm^{-1} were further significantly increased (compared to specimen N20). The reason for this increase is the increase in NaOH dosage that leads to decalcification between silicates and aluminosilicates [51]. This also confirms the XRD results.

3.4.3. $Ca(OH)_2$ Excitation FT-IR Analysis

The result of the FT-IR analysis of GBFS activated by $Ca(OH)_2$ is shown in Figure 4b. Asymmetric tensile vibration of the Si–O–T bond was observed in specimen C20, but the vibration shifted to a lower wavelength (1117 cm^{-1}) and the intensity decreased significantly compared to N20. The asymmetric stretching vibrations of AlO_4^- groups at 603 cm^{-1} and 670 cm^{-1} have also experienced a left shift and a reduction in vibration intensity, while the asymmetric stretching vibrations of H–OH bonds combined with water at 1620 cm^{-1} and 1686 cm^{-1} have also substantially weakened. These results indicate that although $Ca(OH)_2$-activated GBFS can form silicate and aluminosilicate gels, the excitation effect and the formation amount of polymerization products are both far lower than those excited by NaOH [52]. This also explains why the strength of specimen C20 was significantly lower than that of specimen N20 although it can establish strength. The asymmetric stretching vibrations of the -OH bond at 3405 cm^{-1} and 3547 cm^{-1} in specimen C20 were also significantly weakened, which is related to the weaker alkaline environment $Ca(OH)_2$ established compared to NaOH.

With increasing $Ca(OH)_2$ content, the asymmetric tensile vibration of the Si–O–T bond in specimen C40 shifted to a higher wavelength (1120 cm^{-1}) to the right, and the vibration intensity increased slightly compared to that of specimen C20. This result indicates that the increase in $Ca(OH)_2$ content further promoted the formation of calcium silicate gel. At the same time, the asymmetric stretching vibrations of AlO_4^- groups at 602 cm^{-1} and 669 cm^{-1} in specimen C40 also shifted to the right, and the intensity increased significantly. More importantly, the AlO_4^- group at 825 cm^{-1} reappeared, but this characteristic peak did not appear in specimen N20. The bending vibration at 1459 cm^{-1} also reappeared, indicating

a substantial increase in carbonate production (CO_3^{2-}). These results indicate that the increase in $Ca(OH)_2$ content mainly promotes the formation of silicates, aluminosilicates, and carbonates, thereby improving compressive strength [53]. This confirms the XRD research results. The asymmetric stretching vibrations of -OH at 3405 cm^{-1} and 3547 cm^{-1} were significantly enhanced, which is related to the increased $Ca(OH)_2$ dosage.

With further increases of the $Ca(OH)_2$ dosage, the asymmetric tensile vibration of Si–O–T bonds in specimen C60 shifted from the right to 1118 cm^{-1}, and the vibration intensity decreased to a certain extent. At the same time, the asymmetric tensile vibrations of AlO_4^- groups at 603 cm^{-1}, 669 cm^{-1}, and 875 cm^{-1} did not increase further, and the CO_3^{2-} bending vibration at 1458 cm^{-1} did not show a significant increase. However, slight increases in the -OH asymmetric stretching vibrations at 3405 cm^{-1} and 3547 cm^{-1} (compared to specimen C40) were observed, indicating that an increase in the amount of $Ca(OH)_2$ did not promote the formation of silicates and aluminosilicates. $Ca(OH)_2$ precipitated in specimen C60 and enhanced the -OH asymmetric stretching vibration [54]. This result explains the appearance of point-like structures in specimen C60 as observed in SEM.

4. Conclusions

In this study, the influence of a weak-alkali reaction environment on the excitation effect and compressive strength development of alkali GBFS was evaluated. A combination of XRD, SEM, and FT-IR analyses of the micro excitation mechanism under different alkali excitation conditions was used.

(1) The mixing alkalinity of free water or Na_2CO_3 solution is too low and can, thus, only stimulate the free active ions on the GBFS surface to participate in the polymerization reaction. Consequently, only a small amount of silicate or aluminate minerals is generated, which cannot form the gel structure and establish the required compressive strength.

(2) $Ca(OH)_2$ can stimulate the reactivity of GBFS, but the activation effect is lower than that of NaOH, as mainly aluminosilicate minerals are formed (reaching 25.5 MPa after 28 days of curing). With increasing $Ca(OH)_2$ dosage, the excitation effect was substantially enhanced, the formation of aluminosilicate increased, the microstructure improved further, and the mechanical properties also improved. However, excessive addition of $Ca(OH)_2$ will lead to the formation of point-like crystals in the microstructure, thereby affecting the development of mechanical properties.

(3) Although $Ca(OH)_2$-activated GBFS causes a decrease in compressive strength, it substantially reduces preparation costs. This reduction is beneficial for market promotion and engineering applications of alkali-activated materials.

Author Contributions: Software, Z.C.; formal analysis, J.Q.; investigation, J.X.; resources, X.Z.; data curation, Y.H.; writing—original draft preparation, G.H.; writing—review and editing, G.H.; funding acquisition, F.Z. All authors have read and agreed to the published version of the manuscript.

Funding: The research described in this paper was financially supported by Anhui Provincial Natural Science Foundation "Design and Collaborative Enhancement Mechanism of Cement Improved Coal Gangue Alkali Activated Double Cementitious Material" (2308085ME184) and Research and Development Special Project of Environmentally Friendly Materials and Occupational Health Research Institute (Wuhu), Anhui University of Science and Technology "Research and application of compatible coupling and synergistic enhancement mechanism of alkali activated cementitious materials" (ALW2021YF01); 2023 Wuhu Science and Technology Bureau Applied Basic Research Project "Design and Collaborative Enhancement Mechanism of Cement Improved Waste Incineration Bottom Ash Alkali Activated Double Cementitious Materials" (No. 2023jc01); Anhui Provincial Department of Education's 2022 Provincial Quality Engineering Project for Higher Education Institutions "Anhui University of Science and Technology Wuhu Qiuhua Group Practical Education Base" (2022xqhz015); Anhui Provincial Department of Education's 2023 New Era Education Quality Project "Wuhu Qiuhua Thermal Insulation Materials Co., Ltd. Graduate Enterprise Workstation" (2023qygzz021).

Data Availability Statement: Some or all data, models, and code that support the findings of this study are available from the corresponding author upon reasonable request.

Acknowledgments: Thank you to the Analysis and Testing Center of Anhui University of Science and Technology for testing the relevant test samples.

Conflicts of Interest: Author Xiaojun Zheng was employed by the company China Construction Second Engineering Bureau Co., Ltd. Author Fengan Zhang was employed by the Special Equipment Inspection Institute of Anhui.

References

1. Luukkonen, T.; Abdollahnejad, Z.; Yliniemi, J.; Kinnunen, P.; Illikainen, M. One-part alkali-activated materials: A review. *Cem. Concr. Res.* **2018**, *103*, 21–34. [CrossRef]
2. Provis, L.J.; Palomo, A.; Shi, C. Advances in understanding alkaliactivated materials. *Cem. Concr. Res.* **2015**, *78*, 110–125. [CrossRef]
3. Shi, Z.; Shi, C.; Zhang, J.; Wan, S.; Zhang, Z.; Ou, Z. Alkali-silica reaction in water glass-activated slag mortars incorporating fly ash and metakaolin. *Cem. Concr. Res.* **2018**, *108*, 10–19. [CrossRef]
4. Huang, G.; Zhang, X.; Liu, M.; Fang, B.; Wang, C.; Mi, H. Compatibility of sodium hydroxide, sodium silicate and calcium-enriched additives in alkali-activated materials: From the perspectives of flowability, strength and microstructure. *Constr. Build. Mater.* **2023**, *403*, 133102. [CrossRef]
5. Huang, G.; Yang, K.; Sun, Y.; Lu, Z.; Zhang, X.; Zuo, L.; Feng, Y.; Qian, R.; Qi, Y.; Ji, Y.; et al. Influence of NaOH content on the alkali conversion mechanism in MSWI bottom ash alkali-activated mortars. *Constr. Build. Mater.* **2020**, *248*, 118582. [CrossRef]
6. Abdulkareem, M.; Havukainen, J.; Nuortila-Jokinen, J.; Horttanainen, M. Environmental and economic perspective of waste-derived activators on alkaliactivated mortars. *J. Clean. Prod.* **2021**, *280*, 124651. [CrossRef]
7. Ye, H.; Radlińska, A. Shrinkage mitigation strategies in alkali-activated slag. *Cem. Concr. Res.* **2017**, *101*, 131–143. [CrossRef]
8. Huang, G.; Ji, Y.; Li, J.; Hou, Z.; Jin, C. Use of slaked lime and Portland cement to improve the resistance of MSWI bottom ash-GBFS geopolymer concrete against carbonation. *Constr. Build. Mater.* **2018**, *166*, 290–300. [CrossRef]
9. Wang, W.; Noguchi, T.; Tomoyose, A.; Zhang, Y.; Maruyama, I. Influence of volcanic glass powder on alkali-silica reaction expansion in alkali-activated slag mortars. *Cem. Concr. Compos.* **2024**, *152*, 105665. [CrossRef]
10. Huang, G.; Zheng, X.; Gao, M.; Chen, Q.; Qiao, Z.; Xie, T.; Deng, M.; Wei, Q. Mechanical properties and mineral crystal characteristics of multi-source coal-based solid waste filling materials under different proportioning. *Crystals* **2023**, *12*, 470. [CrossRef]
11. Shi, Z.; Shi, C.; Wan, S.; Li, N.; Zhang, Z. Effect of alkali dosage and silicate modulus on carbonation of alkaliactivated slag mortars. *Cem. Concr. Res.* **2018**, *113*, 55–64. [CrossRef]
12. Nasr, D.; Pakshir, A.H.; Ghayour, H. The influence of curing conditions and alkaline activator concentration on elevated temperature behavior of alkali activated slag (AAS) mortars. *Constr. Build. Mater.* **2018**, *190*, 108–119. [CrossRef]
13. Jiao, Z.; Wang, Y.; Zheng, W.; Huang, W. Effect of the activator on the performance of alkali-activated slag mortars with pottery sand as fine aggregate. *Constr. Build. Mater.* **2019**, *197*, 83–90. [CrossRef]
14. Maraghechi, H.; Rajabipour, F.; Pantano, C.G.; Burgos, W.D. Effect of calcium on dissolution and precipitation reactions of amorphous silica at high alkalinity. *Cem. Concr. Res.* **2016**, *87*, 1–13. [CrossRef]
15. Sun, Z.; Vollpracht, A. Isothermal calorimetry and in-situ XRD study of the NaOH activated fly ash, metakaolin and slag. *Cem. Concr. Res.* **2018**, *103*, 110–122. [CrossRef]
16. Puertas, F.; Gonzalez-Fontebo, B.; Gonzalez-Taboada, I.; Alonso, M.M.; Torres-Carrasco, M.; Rojo, G.; Martínez-Abella, F. Alkali-activated slag concrete: Fresh and hardened behaviour. *Cem. Concr. Compos.* **2018**, *85*, 22–31. [CrossRef]
17. *GB/T 203-2008*; Granulated Blastfurnace Slag Used for Cement Production. AQSIQ: Beijing, China, 2008.
18. *GB/T 17671-2021*; Test Method of Cement Mortar Strength(ISO Method). AQSIQ: Beijing, China, 2021.
19. Snellings, R.; Suraneni, P.; Skibsted, J. Future and emerging supplementary cementitious materials. *Cem. Concr. Res.* **2023**, *171*, 107199. [CrossRef]
20. Ding, Y.; Dai, J.-G.; Shi, C.-J. Mechanical properties of alkali-activated concrete: A state-of-the-art review. *Constr. Build. Mater.* **2016**, *127*, 68–79. [CrossRef]
21. Abdalqader, A.F.; Jin, F.; Al-Tabbaa, A. Development of greener alkali-activated cement: Utilisation of sodium carbonate for activating slag and fly ash mixtures. *J. Clean. Prod.* **2016**, *113*, 66–75. [CrossRef]
22. Puertas, F.; Torres-Carrasco, M. Use of glass waste as an activator in the preparation of alkali-activated slag. Mechanical strength and paste characterisation. *Cem. Concr. Res.* **2014**, *57*, 95–104. [CrossRef]
23. Aydın, S.; Baradan, B. Effect of activator type and content on properties of alkali-activated slag mortars. *Compos. Part B Eng.* **2014**, *57*, 166–172. [CrossRef]
24. Chi, M. Effects of dosage of alkali-activated solution and curing conditions on the properties and durability of alkali-activated slag concrete. *Constr. Build. Mater.* **2012**, *35*, 240–245. [CrossRef]
25. Williamson, T.; Juenger, M.C.G. The role of activating solution concentration on alkali-silica reaction in alkali-activated fly ash concrete. *Cem. Concr. Res.* **2016**, *83*, 124–130. [CrossRef]
26. Yang, S.; Poon, C.S.; Cui, H. Alkali-silica reactivity of lightweight aggregates in alkali-activated slag cement and ordinary Portland cement systems. *J. Clean. Prod.* **2023**, *390*, 136187. [CrossRef]

27. Rashad, A.M. A comprehensive overview about the influence of different additives on the properties of alkali-activated slag—A guide for Civil Engineer. *Constr. Build. Mater.* **2013**, *47*, 29–55. [CrossRef]
28. Puertas, F.; Varga, C.; Alonso, M.M. Rheology of alkali-activated slag pastes. Effect of the nature and concentration of the activating solution. *Cem. Concr. Compos.* **2014**, *53*, 279–288. [CrossRef]
29. Fernandez-Jimenez, A.; Puertas, F. Structure of calcium silicate hydrates formed in alkaline-activated Slag: Influence of the type of alkaline activator. *J. Am. Ceram. Soc.* **2003**, *86*, 1389–1394. [CrossRef]
30. Rossen, J.E.; Lothenbach, B.; Scrivener, K.L. Composition of C–S–H in pastes with increasing levels of silica fume addition. *Cem. Concr. Res.* **2015**, *75*, 14–22. [CrossRef]
31. Provis, J.L.; Myers, R.J.; White, C.E.; Rose, V.; van Deventer, J.S.J. X-ray microtomography shows pore structure and tortuosity in alkali-activated binders. *Cem. Concr. Res.* **2012**, *42*, 855–864. [CrossRef]
32. L'Hôpital, E.; Lothenbach, B.; Scrivener, K.; Kulik, D.A. Alkali uptake in calcium alumina silicate hydrate (C-A-S-H). *Cem. Concr. Res.* **2016**, *85*, 122–136.
33. Oh, J.E.; Monteiro, P.J.M.; Jun, S.S.; Choi, S.; Clark, S.M. The evolution of strength and crystalline phases for alkali-activated ground blast furnace slag and fly ashbased geopolymers. *Cem. Concr. Res.* **2010**, *40*, 189–196. [CrossRef]
34. García-Lodeiro, I.; Fern, A.; Palomo, A.; Macphee, D.E. Effect of calcium additions on N–A–S–H cementitious gels. *J. Am. Ceram. Soc.* **2010**, *93*, 1934–1940. [CrossRef]
35. Chindaprasirt, P.; De Silva, P.; Sagoe-Crentsil, K.; Hanjitsuwan, S. Effect of SiO_2 and Al_2O_3on the setting and hardening of high calcium fly ash-based geopolymer systems. *J. Mater. Sci.* **2012**, *47*, 4876–4883. [CrossRef]
36. Dedecek, J.; Lucero, M.J.; Li, C.; Gao, F.; Klein, P.; Urbanova, M.; Tvaruzkova, Z.; Sazama, P.; Sklenak, S. Complex analysis of the aluminum siting in the framework of silicon-rich zeolites. A case study on ferrierites. *J. Phys. Chem. C* **2011**, *115*, 11056–11064. [CrossRef]
37. Hajimohammadi, A.; Provis, J.L.; van Deventer, J.S.J. The effect of silica availability on the mechanism of geopolymerisation. *Cem. Concr. Res.* **2011**, *41*, 210–216. [CrossRef]
38. Zheng, Z.; Ma, X.; Zhang, Z.; Li, Y. In-situ transition of amorphous gels to Na-P1 zeolite in geopolymer: Mechanical and adsorption properties. *Constr. Build. Mater.* **2019**, *202*, 851–860. [CrossRef]
39. Ro, P.; Kr, M.; Mozgawa, W. Geopolymer-zeolite composites: A review. *J. Clean. Prod.* **2019**, *230*, 557–579.
40. Cao, R.; Zhang, S.; Banthia, N.; Zhang, Y.; Zhang, Z. Interpreting the early-age reaction process of alkali-activated slag by using combined embedded ultrasonic measurement, thermal analysis, XRD, FTIR and SEM. *Compos. Part. B Eng.* **2020**, *186*, 107840. [CrossRef]
41. Swanton, S.W.; Heath, T.G.; Clacher, A. Leaching behaviour of low Ca:Si ratio CaO-SiO_2-H_2O systems. *Cem. Concr. Res.* **2016**, *88*, 82–95. [CrossRef]
42. Li, C.; Sun, H.; Li, L. A review: The comparison between alkali-activated slag (Si + Ca) and metakaolin (Si + Al) cements. *Cem. Concr. Res.* **2010**, *40*, 1341–1349. [CrossRef]
43. Du, S.; Zhao, Q.; Shi, X. Quantification of the reaction degree of fly ash in blended cement systems. *Cem. Concr. Res.* **2023**, *167*, 107121. [CrossRef]
44. Irbe, L.; Beddoe, R.E.; Heinz, D. The role of aluminium in C-A-S-H during sulfate attack on concrete. *Cem. Concr. Res.* **2019**, *116*, 71–80. [CrossRef]
45. Dai, X.; Aydin, S.; Yardımcı, M.Y.; Qiang, R.; Lesage, K.; De Schutter, G. Rheology, early-age hydration and microstructure of alkali-activated GGBFS-Fly ashlimestone mixtures. *Cem. Concr. Compos.* **2021**, *124*, 104244. [CrossRef]
46. Huang, G.; Li, Y.; Zhang, Y.; Zhu, J.; Li, D.; Wang, B. Effect of Sodium Hydroxide, Liquid Sodium Silicate, Calcium Hydroxide, and Slag on the Mechanical Properties and Mineral Crystal Structure Evolution of Polymer Materials. *Crystals* **2021**, *11*, 1586. [CrossRef]
47. Rifaai, Y.; Yahia, A.; Mostafa, A.; Aggoun, S.; Kadri, E.H. Rheology of fly ash-based geopolymer: Effect of NaOH concentration. *Constr. Build. Mater.* **2019**, *223*, 583–594. [CrossRef]
48. Gijbels, K.; Pontikes, Y.; Samyn, P.; Schreurs, S.; Schroeyers, W. Effect of NaOH content on hydration, mineralogy, porosity and strength in alkali/sulfate-activated binders from ground granulated blast furnace slag and phosphogypsum. *Cem. Concr. Res.* **2020**, *132*, 106054. [CrossRef]
49. Zhu, Y.; Longhi, M.A.; Wang, A.; Hou, D.; Wang, H.; Zhang, Z. Alkali leaching features of 3-year-old alkali activated fly ash-slag-silica fume: For a better understanding of stability. *Compos. B Eng.* **2022**, *230*, 109469. [CrossRef]
50. Ye, H.; Chen, Z.; Huang, L.E. Mechanism of sulfate attack on alkali-activated slag: The role of activator composition. *Cem. Concr. Res.* **2019**, *125*, 105868. [CrossRef]
51. Wang, J.; Lyu, X.; Wang, L.; Cao, X.; Liu, Q.; Zang, H. Influence of the combination of calcium oxide and sodium carbonate on the hydration reactivity of alkali-activated slag binders. *J. Clean. Prod.* **2018**, *171*, 622–629. [CrossRef]
52. L'hôpital, E.; Lothenbach, B.; Le Saout, G.; Kulik, D.; Scrivener, K. Incorporation of aluminium in calcium-silicate-hydrates. *Cem. Concr. Res.* **2015**, *75*, 91–103. [CrossRef]

53. Abdalqader, A.; Jin, F.; Al-Tabbaa, A. Performance of magnesia-modified sodium carbonate-activated slag/fly ash concrete. *Cem. Concr. Compos.* **2019**, *103*, 160–174. [CrossRef]
54. Dai, X.; Aydın, S.; Yardımcı, M.Y.; Lesage, K.; De Schutter, G. Effects of activator properties and GGBFS/FA ratio on the structural build-up and rheology of AAC. *Cem. Concr. Res.* **2020**, *138*, 106253. [CrossRef]

Disclaimer/Publisher's Note: The statements, opinions and data contained in all publications are solely those of the individual author(s) and contributor(s) and not of MDPI and/or the editor(s). MDPI and/or the editor(s) disclaim responsibility for any injury to people or property resulting from any ideas, methods, instructions or products referred to in the content.